Ultrafast carrier dynamics and resonant inter-miniband nonlinearity of a cubic GaN/AlN superlattice

Thorben Jostmeier,[1] Tobias Wecker,[2] Dirk Reuter,[2] Donat J. As,[2] and Markus Betz[1]
[1]*Experimentelle Physik 2, TU Dortmund University, Otto-Hahn-Straße 4, 44227 Dortmund, Germany*
[2]*Fachbereich Physik, University of Paderborn, Warburger Straße 100, 33098 Paderborn, Germany*

(Received 28 September 2015; accepted 11 November 2015; published online 23 November 2015)

We investigate the linear and dynamical nonlinear optical properties of a superlattice composed of ultra-narrow n-doped GaN/AlN quantum wells. Owing to huge band offsets, the structures feature a broad inter-miniband transition in the telecom window at 1.55 μm. Resonant pump-probe experiments directly reveal ultrafast intersubband relaxation occurring within <100 fs. We estimate an associated third order nonlinear optical susceptibility of $\mathrm{Im}(\chi^{(3)}) \sim 1.1 \times 10^{-20}$ m^2/V^2. The polarization and angular dependences of the optical response confirm the nonlinearity as originating from inter-miniband transitions in the heterostructure. © *2015 AIP Publishing LLC*.
[http://dx.doi.org/10.1063/1.4936330]

Intersubband (ISB) transitions in semiconductor quantum wells (QWs) feature a broad variety of interesting linear and nonlinear optical properties. Owing to the huge conduction band offsets between the different III-V-nitrides, the transition energy in thin GaN/AlN QWs can be tuned towards the near-infrared and, ultimately, even into the telecom window. Consequently, a number of studies have elucidated the dynamical optical nonlinearity of such nitride based heterostructures.[1–7] So far, these experiments have focused on the common hexagonal structural phase. While this phase is widely used for nitride based devices, it is characterized by the presence of strong spontaneous and piezoelectric polarizations along the c-axis. For heterostructures, the resulting internal electric fields complicate the design as they, e.g., separate electrons and holes and, thereby reduce the luminescence yield. Much less effort has been devoted to zincblende GaN and AlN. While this cubic phase is more challenging to grow, its heterostructures are intrinsically devoid of internal polarization fields along the QW growth direction. Recently, ISB transitions in the near-infrared have been achieved in n-doped GaN/AlN QWs fabricated by plasma-assisted molecular beam epitaxy (PA-MBE).[8,9] Studies of the ultrafast carrier dynamics or the nonlinear optical properties of these cubic heterostructures have not been reported so far. This gap is closed by the present letter, where we present a detailed analysis of the optical properties of a cubic GaN/AlN superlattice with inter-miniband (IMB) transitions in the near-infrared. The study comprises measurements of the linear optical properties and pump-probe studies in various configurations. As the main result, we extract the magnitude of the nonlinear optical susceptibility associated with the IMB transitions.

For heterostructure growth, we use a PA-MBE system (Riber-32). While it is equipped with standard effusion cells for the evaporation of Ga and Al, atomic nitrogen is provided by a plasma source (Oxford). The growth process is controlled *in situ* by reflection high energy electron diffraction. A 10 μm 3C-SiC (001) epilayer on a 0.5 mm thick Si substrate serves as a substrate for epitaxial growth. It is held at a temperature of 720 °C. Details about the growth of cubic GaN on 3C-SiC can be found in Ref. 10. Heterostructure growth starts with the deposition of a 100 nm thick cubic GaN layer. The superlattice consists of 80 periods of nominally 1 nm thick AlN barriers and nominally 1.8 nm thick n-doped GaN QWs (cf. illustration in Fig. 1(a)). Si with a concentration of $\sim 10^{19}$ cm^{-3} acts as a dopant. Atomic force microscopy reveals a typical rms surface roughness of $\sim$6 nm over a 10 × 10 μm^2 area.

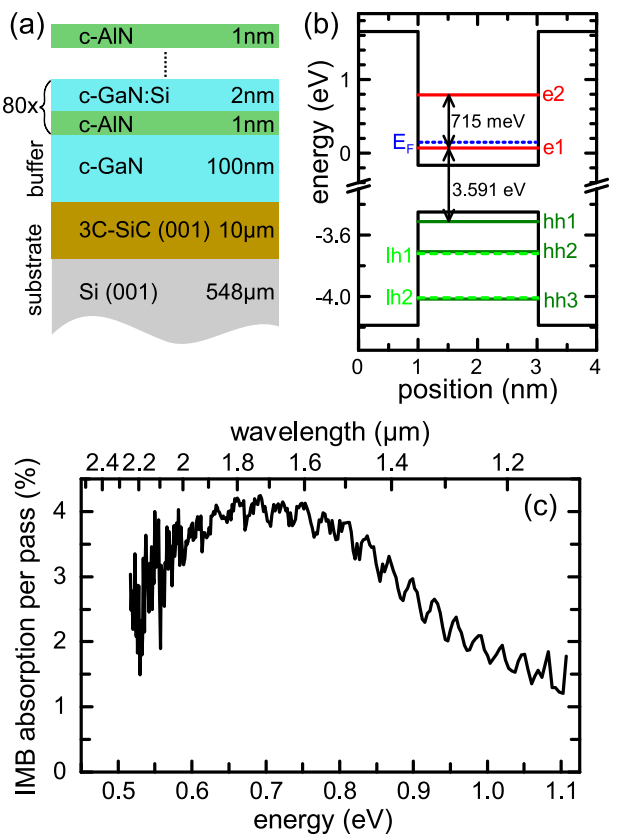

FIG. 1. (a) Layer sequence of the cubic GaN/AlN superlattice. (b) Simulation of the energy levels of a single QW. The energies of the ISB and the interband transition are visualized by vertical arrows. e: conduction subbands, hh: heavy hole, lh: light hole. (c) Spectrally resolved IMB absorption per pass through the superlattice.

We first address the linear optical properties of the superlattice by analyzing its near-infrared absorption. In general, ISB transitions are driven by electric field components along the growth direction. The most pronounced interaction would, therefore, occur for TM polarized light propagating parallel to the superlattice layers. Here, instead, the interaction is maximized by multiple reflections in a waveguide geometry. The side facets of the waveguide are tilted by 30° with respect to the surface. Light incident on these side facets undergoes total internal reflection at both the Si-air and the superlattice-air interface. Specifically, it experiences ~20 reflections at the superlattice-air side with an angle of incidence of ~43° (cf. inset of Fig. 2 for visualization). Note that IMB absorption is expected for TM polarized light only. The IMB absorption is quantified by spectrally resolving the different transmissions of TM and TE polarized light through the waveguide. To this end, a stable tungsten light source and a monochromator equipped with an InGaAs photodiode is used. For reference purposes, a waveguide containing a 600 nm epilayer of cubic GaN instead of the superlattice is analyzed. All experiments are performed at room temperature.

Fig. 1(c) displays the result for the IMB absorption spectrum normalized by the number of passes through the superlattice. The data are extracted from the different TM and TE transmissions through the waveguide structure normalized to the respective results for the reference sample. The accessible photon energy range is $0.5\,\text{eV} \leq \hbar\omega \leq 1.1\,\text{eV}$ limited by the detector and the absorption of silicon, respectively. Most strikingly, we find a strong and broad IMB transition centered at ~0.7 eV. The additional spectral oscillations are related to Fabry-Perot fringes of the 10 μm thick SiC layer. Remarkably, the width of the IMB transition is as large as ~370 meV (FWHM), whereas, in previous studies on cubic[8,9] or hexagonal[11–13] GaN/Al(Ga)N heterostructures, this width did not exceed 240 meV. We attribute the enormous transition width to two mechanisms: (i) The ultranarrow AlN barriers enhance the tunnel coupling between adjacent quantum wells and, thereby substantially broaden the resulting minibands. (ii) Our structures exhibit monolayer fluctuations of the quantum well widths. It has been shown that such surface roughness leads to substantial broadening of ISB transitions.[14–16] It is also possible that the linewidth is further increased by spatial inhomogeneities across the macroscopic waveguide.

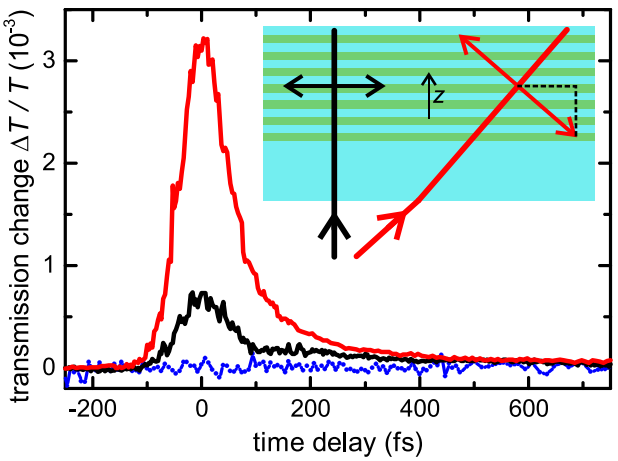

FIG. 2. Pump induced change of the transmission of the superlattice for a central photon energy of 0.82 eV and a pump irradiance of 36 GW/cm^2. Red: angle of incidence 65°, TM polarization. Black: close-to-normal incidence. The geometries are illustrated in the inset. The blue dotted line corresponds to TE polarized pulses (angle of incidence 65°).

For a more quantitative understanding of the optical transitions, numerical simulations for the band structure are performed. As a useful starting point, we calculate the energy level structure of single GaN/AlN QWs with the commercial Schrödinger-Poisson solver nextnano^3 (Ref. 17) with material parameters taken from Ref. 18. In Fig. 1(b), the energy level scheme of a single QW at 300 K is shown. The best match of the theoretical ISB transition energy to the experimentally observed IMB transition is achieved assuming a 2.025 nm thick QW. It is, therefore, likely that the QWs in the superlattice are ~1 monolayer thicker than nominally intended. However, for a more thorough theoretical understanding, the simulation would have to treat the actual superlattice instead of a single QW. The simulation also permits to predict interband transitions of the heterostructure. The energetically lowest transition is found at $E_{inter}^{theory} = 3.591\,\text{eV}$. This value is very close to the maximum of the photoluminescence observed at $E_{PL}^{exp} = 3.532\,\text{eV}$ (data not shown). Note that the nextnano^3 simulation does not account for the substantial exciton binding energy. In cubic bulk GaN, this exciton binding energy is as large as $E_{ex}^{bulk} = 24\,\text{meV}$.[19] It should further increase to $E_{ex}^{QW} = 48\text{meV}$ in a ~2 nm wide QW.[20]

We now turn towards the central aspect of this study which is the analysis of the ultrafast and nonlinear dynamical response of the IMB transitions. To this end, we use a degenerate femtosecond pump-probe setup. Geometrical restrictions of such a two-beam experiment inhibit the use of the above waveguide geometry. Instead, we investigate a single pass through the heterostructure far away from normal incidence. To eliminate the influence of the optical nonlinearity of the silicon substrate, the sample is glued onto a fused silica window. The silicon is then removed mechanically. As a result, the GaN/AlN superlattice is effectively sandwiched between the SiC layer and the fused silica substrate, i.e., dielectrics with rather small optical nonlinearity. To quantify this residual nonlinearity, we also process a reference sample based on a bare SiC/Si wafer and use it to single out effects caused by the SiC or SiO_2 layers.

The light source for the pump-probe experiments is an optical parametric amplifier (Coherent OPA 9850). It emits ~50 fs pulses at 250 kHz repetition rate. The central wavelength is tunable from 1375 nm (0.8 eV) to 1550 nm (0.9 eV), i.e., close to the center of the IMB resonance. Pump and probe pulses are focused to a ~50 μm spot (FWHM) with a relative angle of ~10°. The normalized pump-induced change $\Delta T/T$ of the probe transmission is measured with lock-in detection referenced to the excitation. The pump-probe data below are averaged over several scans, and the signals of the reference sample are subtracted from the transients obtained in the superlattice sample. To address the IMB transitions, pump and probe beams are TM polarized and the sample is tilted to an angle of incidence of ~65° which, at the same time, is close to the Brewster angle. A

variation of the angle of incidence and the polarizations provide additional means to confirm the optical response of the superlattice sample to originate from the IMB transitions. To provide a benchmark for the actual time-resolution of the setup, we perform intensity autocorrelations based on transient signals related to two-photon absorption in a thin GaAs wafer.

Fig. 2 compares the pump-probe transients for different configurations. All data are obtained with pulses of 0.82 eV central photon energy, i.e., close to the peak of the IMB absorption. In the situation where a strong IMB excitation is expected (cf. red curve, TM polarized light, angle of incidence 65°), a transmission increase of 3×10^{-3} is seen. This transient response arises from a substantial Pauli blocking of the IMB transition. From the data in Fig. 1(c) we estimate a total IMB absorption of $\approx 1.7\%$ for the present geometry (note that the strong refraction at the air-SiC interface leads to a reduced internal angle of incidence of ∼24°). As a result, the transient signal seen in Fig. 2 points to a remarkable change of the IMB absorption strength of nearly 20%. The temporal evolution of the transmission change gives insight into the timescales of the intersubband electron dynamics. The signal decrease following the overlap peak can be roughly fitted by an exponential decay with a time constant of ∼80 fs, reflecting the relaxation into the lowest miniband. This time scale is in fair agreement with theoretical calculations for ISB relaxation[1–3] which predict electron-phonon scattering times of ∼100 fs. Earlier reports on hexagonal GaN/Al(Ga)N multi-QW structures identified relaxation times ranging from 130 fs to 370 fs.[2–5] The faster relaxation times measured here are in part related to the improved temporal resolution of our setup. Note, that we see a residual signal decaying on timescales ∼1–5 ps which, previously, has been attributed to electron thermalization.[2,3] It is also possible that they originate from multi-photon absorption in SiC as the reference sample shows similar signatures.

We now compare the above results to two configurations where the IMB transitions are expected to be inhibited. First we analyze close-to-normal incidence of pump and probe beams (cf. black line in Fig. 2). To compensate for the smaller spotsize, the pump power is lowered such that the irradiance is kept constant. This configuration results in a marked decrease of the transient signal. We attribute the remaining signal to surface roughness and light scattering from the rough interfaces. Roughness is known to partially relax the optical selection rules and to, thereby, slightly allow for otherwise forbidden transitions.[16] In a second set of experiments, we again use an angle of incidence of 65° but change the probe beam to TE polarization (cf. blue dotted line). As expected, no significant pump-induced changes are found.

In the next step, we analyze the spectral dependence of the transients associated with IMB carrier dynamics. Note that the tuning range of our laser system does not permit to cover the entire absorption resonance seen in Fig. 1(c). In particular, we perform degenerate pump-probe measurements while the geometry is kept at an angle of incidence of 65° and TM polarization. As the pulses durations slightly change with wavelength, intensity autocorrelations are measured for the different pulses. Fig. 3 displays exemplary

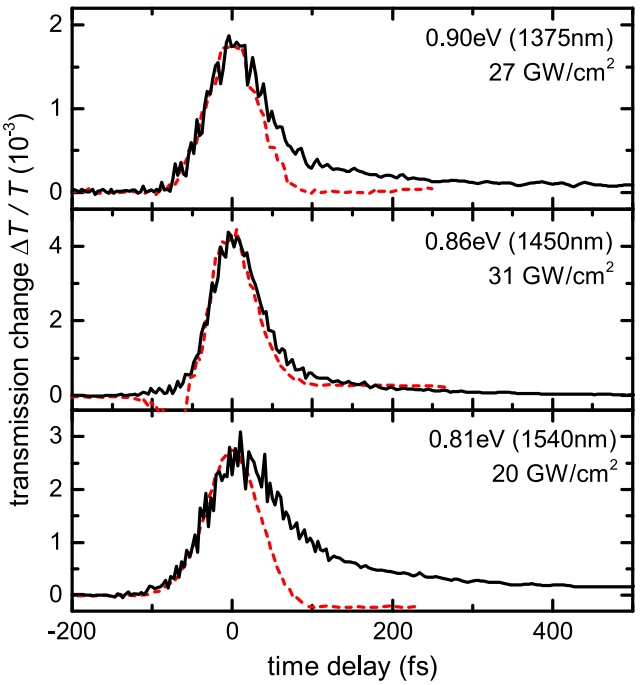

FIG. 3. Pump-probe transients for different central photon energies. The angle of incidence is 65° and the pulses are TM polarized. The red dashed lines are intensity autocorrelations of the pump and probe pulses.

pump-pobe transients. From the top to the bottom panel, the photon energies move closer to the peak of the IMB absorption. The IMB relaxation times are again extracted by fitting a single exponential decay to the data after the overlap peak. No significant deviation from a ∼80 fs decay time is found, which indicates a rather universal IMB dynamics in the investigated regime. The maximum amplitudes of the pump-induced changes do not strictly follow to the spectral dependence of the IMB absorption strength. We attribute this finding partially to the spatial inhomogeneity of the sample. Finally, we turn towards an estimation of the resonant third-order nonlinear susceptibility $\chi^{(3)}$ associated with the IMB transitions. In Fig. 4, the maximum transmission change at nominally zero time delay is plotted versus the irradiance of pump pulses of 0.81 eV central photon energy. The data points nicely follow a linear fit, which indicates that the

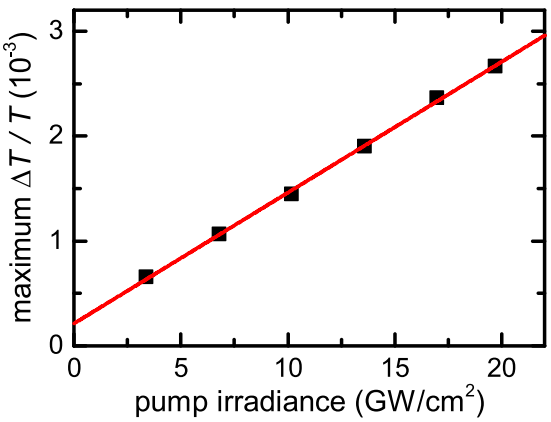

FIG. 4. Dependence of the peak pump-probe signals on the pump irradiance (central photon energy 0.81 eV, TM polarization, 65° angle of incidence). The red line is a linear fit.

absorption of the pump pulse does not yet markedly saturate. In the language of nonlinear optical susceptibilities, this finding implies that the pump-probe measurements are restricted to the $\chi^{(3)}$ regime. We note that the pump power has no significant influence on the temporal shape of the transients.

The magnitude of the third-order nonlinear optical susceptibility is estimated according to the procedure suggested by Hamazaki *et al*.[5] First, we calculate the irradiance level I_s which corresponds to the irradiance required to completely block the absorption of a two-level system approximating the IMB transition. It is given by $I_s = \alpha L/m$ where α is the IMB absorption coefficient, L is the interaction length and $m = 1.25 \times 10^{-4}\text{cm}^2/\text{GW}$ is the slope of the linear dependence seen in Fig. 4. The optical density $\alpha L = 0.017$ is taken from Fig. 1(c) but corrected for the smaller angle of incidence in the pump-probe geometry. Those parameters imply $I_s = 136\,\text{GW}/\text{cm}^2$. To extract $\chi^{(3)}$, we use the relation between the third-order and the linear susceptibility of a two-level system[21]

$$\text{Im}\chi^{(3)} = \frac{-\text{Im}\chi^{(1)}}{3|E_s|^2}, \tag{1}$$

where $|E_S|$ is the field strength at the saturation irradiance I_S. The linear susceptibility $\text{Im}\,\chi^{(1)}$ is extracted from the real part of the refractive index ($\text{Re}(n) = 2.3$) and the absorption coefficient. The resulting third order susceptibility is $\text{Im}\,\chi^{(3)} \sim 1.1 \times 10^{-20}\ \text{m}^2/\text{V}^2$. This value is 1–2 orders of magnitude smaller than previously reported values based on experiments with hexagonal GaN/AlN multi-quantum wells.[5,22] There is room, however, to increase the nonlinearity by engineering narrower IMB resonances and, to some extent, by stronger doping. We also note that this estimate for $\chi^{(3)}$ yields an effective value for the present geometry. In particular, the tensor element of $\chi^{(3)}$ related to pulses propagating along the superlattice layers would be a factor of $\sim(2.5)^4$ larger.

In conclusion, we have analyzed the resonant optical nonlinearity associated with IMB transitions in cubic GaN/AlN superlattices with ultrafast pump-probe spectroscopy. The results reveal a substantial and broadband $\chi^{(3)}$-nonlinearity with <100 fs response time. Such structures would be particularly useful in combination with plasmonic metasurfaces fully exploiting the advantages of ISB transitions for functional nonlinear optical devices.[7,23]

This work has been supported by the collaborative research center SFB TRR 142 of the DFG.

[1]N. Suzuki and N. Iizuka, Jpn. J. Appl. Phys., Part 1 **37**, L369 (1998).
[2]C. Gmachl, S. V. Frolov, H. M. Ng, S. N. G. Chu, and A. Y. Cho, Electron. Lett. **37**, 378 (2001).
[3]J. D. Heber, C. Gmachl, H. M. Ng, and A. Y. Cho, Appl. Phys. Lett. **81**, 1237 (2002).
[4]N. Iizuka, K. Kaneko, and N. Suzuki, Electron. Lett. **40**, 962 (2004).
[5]J. Hamazaki, S. Matsui, H. Kunugita, K. Ema, H. Kanazawa, T. Tachibana, A. Kikuchi, and K. Kishino, Appl. Phys. Lett. **84**, 1102 (2004).
[6]M. J. Karimi and H. Vafaei, Superlattices Microstruct. **78**, 1 (2015).
[7]O. Wolf, A. A. Allerman, X. Ma, J. R. Wendt, A. Y. Song, E. A. Shaner, and I. Brener, Appl. Phys. Lett. **107**, 151108 (2015).
[8]E. A. DeCuir, E. Fred, M. O. Manasreh, J. Schörmann, D. J. As, and K. Lischka, Appl. Phys. Lett. **91**, 041911 (2007).
[9]H. Machhadani, M. Tchernycheva, S. Sakr, L. Rigutti, R. Colombelli, E. Warde, C. Mietze, D. J. As, and F. H. Julien, Phys. Rev. B **83**, 075313 (2011).
[10]J. Schörmann, S. Potthast, D. J. As, and K. Lischka, Appl. Phys. Lett. **90**, 041918 (2007).
[11]A. Helman, M. Tchernycheva, A. Lusson, E. Warde, F. H. Julien, Kh. Moumanis, G. Fishman, E. Monroy, B. Daudin, D. Le Si Dang, E. Bellet-Amalric, and D. Jalabert, Appl. Phys. Lett. **83**, 5196 (2003).
[12]X. Y. Liu, P. Holmström, P. Jänes, L. Thylen, and T. G. Andersson, Phys. Status Solidi B **244**, 2892 (2007).
[13]M. Tchernycheva, L. Nevou, L. Doyennette, F. H. Julien, E. Warde, F. Guillot, E. Monroy, E. Bellet-Amalric, T. Remmele, and M. Albrecht, Phys. Rev. B **73**, 125347 (2006).
[14]J. B. Khurgin, Appl. Phys. Lett. **93**, 091104 (2008).
[15]A. Y. Song, R. Bhat, P. Bouzi, C. Zah, and C. F. Gmachl, e-print arXiv:1507.06016.
[16]R. M. Kemper, P. Veit, C. Mietze, A. Dempewolf, T. Wecker, F. Bertram, J. Christen, J. K. N. Lindner, and D. J. As, Phys. Status Solidi C **12**, 469 (2015).
[17]S. Birner, S. Hackenbuchner, M. Sabathil, G. Zandler, J. A. Majewski, T. Andlauer, T. Zibold, R. Morschl, A. Trellakis, and P. Vogl, Acta Phys. Pol. A **110**, 111 (2006).
[18]T. Wecker, F. Hörich, M. Feneberg, R. Goldhahn, D. Reuter, and D. J. As, Phys. Status Solidi B **252**, 873 (2015).
[19]M. Feneberg, M. Röppischer, C. Cobet, N. Esser, J. Schörmann, T. Schupp, D. J. As, F. Hörich, J. Bläsing, A. Krost, and R. Goldhahn, Phys. Rev. B **85**, 155207 (2012).
[20]H. Mathieu, P. Lefebvre, and P. Christol, Phys. Rev. B **46**, 4092 (1992).
[21]R. W. Boyd, *Nonlinear Optics* (Academic Press, New York, 1992), p. 205.
[22]R. Rapaport, G. Chen, O. Mitrofanov, C. Gmachl, H. M. Ng, and S. N. G. Chu, Appl. Phys. Lett. **83**, 263 (2003).
[23]J. Lee, M. Tymchenko, C. Argyropoulos, P.-Y. Chen, F. Lu, F. Demmerle, G. Boehm, M.-C. Amann, A. Alu, and M. A. Belkin, Nature **511**, 65 (2014).